Bulletin of the Mineral Research and Exploration

http://bulletin.mta.gov.tr

Efficiency of singularity and PCA mapping of mineralization-related geochemical anomalies: a comparative study using BLEG and <180µm stream sediment geochemical data

Fatma Nuran SÖNMEZ[a*], Simay KOÇKAR[a] and Hüseyin YILMAZ[a]

[a]*Dokuz Eylül University, Faculty of Engineering, Department of Geological Engineering, Tınaztepe, Buca, 35160, İzmir, Türkiye*

Research Article

Keywords:
Singularity Mapping, C-A, N-S, PCA, Multi-Fractal Models, Eskişehir.

ABSTRACT

In gold (Au) exploration, the analysis of both bulk leach extractable gold (BLEG) and acid-extractable Au in the <180µm stream sediment fraction are the two most common approaches. The Eskişehir-Sivrihisar region in Western Türkiye hosts several orogenic type mineral deposits. The purpose of this study is to delineate geochemical anomalies of ore-related elements and track their dispersion, which may lead to discovery of unknown ore deposits. This research also compares the capability of conventional statistical and principal component analysis (PCA), with concentration area (C-A) and number-size/concentration (N-S/C) fractal methods as well as singularity index method to differentiate anomalous and background Au distributions. Known Au mineralization in the region of interest is strongly reflected in stream sediment BLEG Au patterns, which have robust singularity indices with C-A and N-S multifractal modeling and PCA. A hundred % of the Au deposits were detected using either BLEG Au and Ag singularity index mapping with C-A fractal analysis whereas the factor analysis of which revealed 85% efficiency. Several strong Au-Ag anomalies defined by the singularity index and factor analysis in this study requires further follow up for the discovery of new deposits.

Received Date: 03.02.2021
Accepted Date: 15.06.2021

1. Introduction

Identification of significant mineralization-related geochemical patterns or anomalies is of great importance in ore deposit exploration. Several statistical methods have been investigated for generating robust geochemical anomaly maps and models from geochemical exploration data. These include conventional parametric and non-parametric methods (Sinclair, 1991; Govett et al., 1975), and alternative techniques that are not dependent on data distribution types or affected by the presence of outlying populations including fractal modelling (Mandelbrot, 1983; Cheng et al., 1996; Afzal et al., 2011; Zuo, 2011; Sadeghi et al., 2015) and catchment basin analysis (Bonham-Carter et al., 1987; Carranza, 2010*a*). In recent years there has been a move towards latter as a more robust approach in the recognition of significant geochemical anomalies (Cheng et al., 1994; Grunsky, 2007, 2010; Carranza, 2010*b*; Zuo and Wang, 2016). In relation, there is also the need to consider spatial patterns and other processes that can lead to complexity in defining geochemically anomalous behavior (Zuo et al., 2013; Parsa et al., 2017*a*; Yılmaz et al., 2019). Explatory Data Analysis (EDA) methods are not as robust as fractal modelling

Citation Info: Sönmez, N. F., Koçkar, S., Yılmaz, H. 2022. Efficiency of singularity and PCA mapping of mineralization-related geochemical anomalies: a comparative study using BLEG and <180mm stream sediment geochemical data. Bulletin of the Mineral Research and Exploration 168, 11-33. https://doi.org/10.19111/bulletinofmre.955280

**Corresponding author: Fatma Nuran SÖNMEZ, nuran.sonmez@deu.edu.tr*

in case of sparse geochemical data. Most EDA methods ignore spatial relations between geochemical data whereas fractal modelling can be designed so as to consider spatial relationships between regolith geochemistry and known mineral deposits (Agterberg et al., 1990).

Fractal modelling uses the complete geochemical data set without the necessity of transformations to meet assumptions about data distribution and effects of outliers (Luz et al., 2014). Fractal modelling is predicted on power-law distribution, which means that some statistical characteristics of the data are invariant (self-similar) at different scales (Mandelbrot, 1983; Shen and Cohen 2005). Fractal models that have gained a considerable application in delineating geochemical anomalies are the number-size (N-S) concentration-area (C-A), singularity indexes (SI) and concentration-volume (C-V) (Mandelbrot, 1983; Cheng et al., 1996, 2000; Cheng, 2007; Afzal et al., 2010; Daneshvar, 2017; Yasrebi and Hezarkhani, 2019; Zadmehr and Shahrokhi, 2019; Aliyari et al., 2020; Mirzaie et al., 2020; Ahmadi et al., 2021). Afzal et al. (2013) delineated different Au mineralized zones in the Qolqoleh orogenic gold deposit by the C–V fractal model. They emphasized that extremely highly mineralized Au zones identified by the C–V fractal model had a positive correlation with meta-volcanic rocks whereas moderately mineralized zones correlate with sericite schist in the Qolqoeh (Iran) deposit. Similarly, Mirzaie et al. (2020) determined the zones based on ores and gangues by using a combination of fractal and factor analysis in the Chah Gaz iron ore (Central Iran). They successfully differentiated waste material from ore zones for proper exploitation. In other words, the C-V fractal modeling, which has been used for the classification of different populations including parameters such as regionalized variables of environment and economy used to identify zones of mineralization in various ores (Mirzaie et al., 2020). Zadmehr and Shahrokhi (2019) has re-discovered Qolqoleh, Kervian and Qabaghloujeh (Iran) Au deposits using concentration-area (C-A) and concentration-number (C-N)-categorized Au, As, Hg and Bi anomalies. They showed that C-A and C-N fractal-modeled anomalous results had a very strong correlation with rock units including highly deformed acidic and basic metavolcanic and sericite schists. Shuguang et al. (2015) has classified fractal or multifractal approaches employed in geochemical anomaly definition into hard- and soft-threshold techniques. The hard-threshold group includes N-S and C-A fractal models with clear-cut thresholds to define population breaks and identify anomalies but fails to identify more subtle changes in fractal behavior typical of complicated or composite geological environments (Zuo et al., 2013). The soft-threshold methods include S-A and SI multifractal techniques. These filtering methods improve the reliability in setting thresholds for geochemically anomalous populations but are unable to determine thresholds for the separation of geochemical populations (Zuo and Wang, 2016). Thus, geochemical signatures generated by the S-A and singularity mapping methods essentially require additional calibration of geochemical values to adjust for potential dilution effects following the concepts of Hawkes (1976). For stream sediment geochemistry sediment dilution in drainage must also be taken into account as a potential factor in setting thresholds to background Au distributions. The typical approach is to use catchment area weighting This study compares the results of selected conventional and fractal methods to define anomalous catchments based on both raw and catchment-weighted BLEG Au and Ag values well as <180µm Au, Ag, Cu, Pb, Zn, As and Sb values. Verification of the results attained can be employed utilizing geochemical properties of already discovered gold deposits and prospects along with the rock chip samples in the area.

2. Study Area and Data

2.1. Regional Geology and Tectonic Setting

The study area of ~2.662 km^2 is situated in the Eskisehir region of Western Türkiye. It is underlain by three major ore-hosting tectono-stratigraphic units (Figure 1). These are: a) the Precambrian to Lower Paleozoic undifferentiated high-grade unit consisting of gneiss, metagranite, schist, amphibolite and marble, which are cut by Upper Paleozoic granitoids; b) the Triassic Karakaya Complex containing low-grade schists and marbles with meta-sandstone, meta-mudstone, and meta-volcanic/volcanic intercalations (Altıner et al., 1991; Okay et al., 1996) and c) Jurassic-Cretaceous ophiolites or accretionary meta-clastic rocks intruded by Cenozoic magmatic units (Okay and Satır, 2000; Yılmaz, 2003). The low-grade schists and

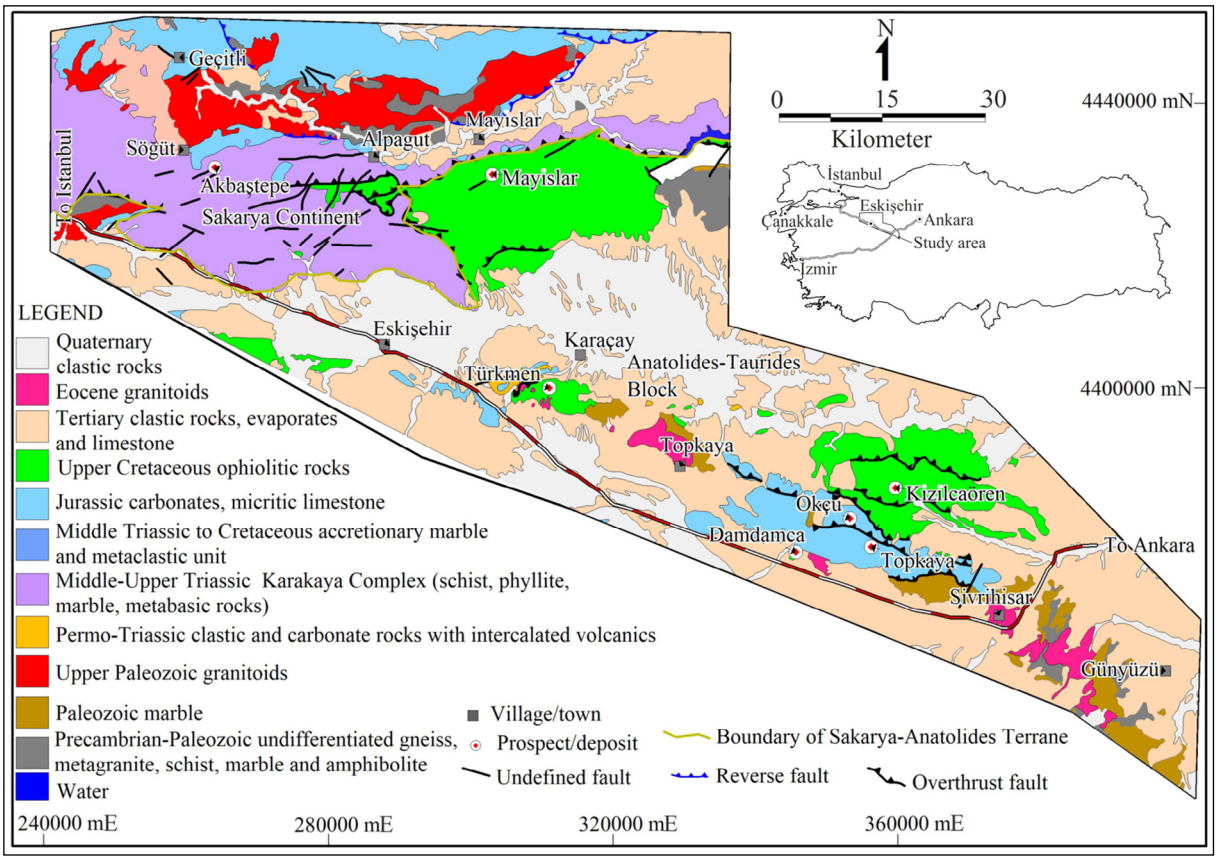

Figure 1- Simplified geological map of the Karakaya Formation, Cenozoic volcano- plutonic field and sedimentary cover rocks in Eskişehir-Sivrihisar region, location of the study area and significant mineralizations (after Okay et al., 1996; Okay and Satır, 2000; MTA, 2002; Yılmaz, 2003 and this study).

marbles are considered parts of the Karakaya Complex (Okay et al., 1996). The Karakaya Complex contains metamorphosed mafic rocks, which are intercalated with phyllite and marble, and was strongly affected by Alpine north-south-trending compressional tectonics during the Upper Cretaceous-Eocene.

2.2. Local Geology and Mineralization

The Karakaya Complex hosts the probable orogenic-type Akbaştepe Au-As-Sb-W deposit (SE of Söğüt; MTA, 1965, 1970; Yılmaz, 2003), as well as the epithermal-style Damdamca and Topkaya Au-Ag deposits to the NW of Sivrihisar, and the Mayıslar and Türkmen deposits (Table 1). In the Akbaştepe deposit, Au mineralization is contained in quartz veins, with peak grades of 20 g/t Au over a 220 m strike length and width of 2 m (Eurogold, 1996) in low- grade schists and marbles. The Damdamca and Topkaya Au-Ag-As deposits have a combined indicated resource of 1.454 Mt at 4.07 g/t Au, and a resource of 1.950 Mt at 4.9 g/t Au (Koza Gold, 2013). The Damdamca deposit is hosted in a serpentinite block, being sandwiched between the Damdamca granite and meta-clastic rocks whereas the Topkaya deposit is hosted in marble and meta-clastic rocks. Both deposits occur in the footwall of a south-verging thrust (Yılmaz, 2003).

The sub-economic Mayıslar polymetallic Cu-Pb-Zn-As-Mo is hosted in Eocene andesite and tectonically emplaced Cretaceous ophiolites (Parlak and Sayılı, 2012). In the deposit, altered (silicified, seriticized, argillized) andesites, which are enriched in tourmaline, are intersected by quartz and calcite veins. According to Parlak and Sayılı (2012), the alteration mineralogy is characterized by the presence of high temperature quartz and sericite forming between 270 and 370 °C and, sericite. The ore mineralogy and the presence of tourmaline suggest the possibility of a buried granitoid intrusion somewhere at depth (Parlak and Sayılı, 2012).

Table 1- Characteristics of and reserve or resource data for orogenic precious/base metal deposits and prospects in Eskişehir-Sivrihisar region, Western Türkiye.

Name	Commodity	Tectonic belt	Host rock	Deposit Type	Age of host rock	Ore body and Structure	Mineral reserve/resources	Status	Reference
Türkmen	Pb, Zn, Ag, Cu, As, Mo	Anatolid-Taurid	Granodiorite, monzodirite porphyry	Epithermal (Orogenic)	Eocene	Not known	Very significant Cu, Pb, Zn, Ag, Mo, As in soil	Prospect	Yılmaz, 2003
Mayıslar	Pb, Zn, Ag, Cu, As, Mo, Sb	Karakaya	Diorite porphyry, microdiorite	Porphyry (intrusion-related)	Eocene	Quartz veinlet	0.5 g/t Au (grab sample)	Prospect	Parlak and Sayılı, 2012
Kızılcaören	REE, Th, Ag	Anatolid-Taurid	Metasandstones, pyroclastics, trachytic porphyry, phonolites	Epithermal (volcanogenic)	Oligo-Miocene	Infilling of radial circular and funnel shaped fractures and five breccia pipes with fluorite, barite and REE	30 Mt@3.14% REE, 37.44% CaF2,31.04% BaSO4; 0.384 Mt@0.212% ThO2 in bastnasite	Prospect	Özgenç, 1993
Okcu	Ag	Anatolid-Taurid	Marble, metaclastic, metacarbonate	Epithermal (Orogenic)	Mesozoic	Silicified carbonates, metacarbonate	Rockchip (max): 11 g/t Ag	Prospect	Eurogold, 1996
Damdamca	Au, Ag, As	Anatolid-Taurid	Marble, metaclastic, metacarbonate	Epithermal (Orogenic Listwanite)	Mesozoic	Quartz vein/veinlet, breccia and replacement in silica-carbonate altered ophiolitic rocks associated with EW-trending thrust faults and shearings	Resource indicated: 1.454 Mt@ 4.07 g/t Au, 4.98 g/t Ag; Resource indicated and inferred: 1.950 Mt@ 4.9 g/t Au, 4.49 g/t Ag	Operating Mine	Koza Gold, 2013
Topkaya	Au, Ag, As	Anatolid-Taurid	Marble, metaclastic, metacarbonate	Epithermal (Orogenic Listwanite)	Mesozoic	Quartz vein/veinlet, breccia and replacement in silica-carbonate altered ophiolitic rocks associated with EW-trending thrust faults and shearings	Included in the above resource	Operating Mine	Koza Gold, 2014
Akbaştepe	Au, As, Sb, W	Upper Paleozoic metamorphic schists and marble	Sakarya continent	Mesothermal (Orogenic)	Permo-Triassic	Quartz vein/veinlet, breccia and replacement in carbonate rocks associated with EW-trending thrust faults and shearings	Resource indicated: 1.943 Mt@ 12.5 g/t Au; Resource inferred: 2.788 Mt@ 10.5 g/t Au, with 1.5 Moz contained Au	Developing Mine	Koza Gold, 2016; AK yatırım report, 2018

The Türkmen deposit is located 6 km north of Türkmentokat village and is underlain by Upper Cretaceous ophiolites intruded by Eocene granodiorite porphyries. Altered serpentinite hosts quartz stockwork containing abundant sphalerite, galena and pyrite, and minor chalcopyrite and arsenopyrite (Eurogold, 1996; Yılmaz, 2003). An Fe-oxide-altered silica cap overlies the intrusive rocks. The Türkmen mineralization has similarities with porphyry intrusive-related skarn systems containing a proximal Pb-Zn-Ag-Cu±Au-Mo-W), peripheral Au-Zn-Pb-As, and distal Pb-Zn-Ag-Au skarn replacements (Yılmaz, 2003). However, proximal or distal skarn alteration and metal-bearing stockwork quartz veins/veinlets in the porphyry intrusions or serpentinites has not been recognized yet.

3. Sampling and Chemical Analysis

A total of 258 BLEG, 612 - <180µm stream sediment and 65 rock chip samples were obtained from the Sivrihisar-Eskişehir region. BLEG sampling was conducted at a density of ~1 sample per 10 km^2 depending on stream system morphology, with sites selection designed to exclude sediment input from higher order streams (Figure 2). The BLEG results were followed up by collecting -180um stream sediment samples from higher order streams at a density of 4 samples per square km. Sampling and analytical techniques as well as precision set by Eurogold according to Howarth (1983) for BLEG and 180µm stream sediment were discussed in detail by Yılmaz et al. (2019) and therefore, the reader is referred to the article cited hereby. Digital geology was provided by MTA (2002). Singularity mapping was carried out by using A MATLAB-based code. C-A and N-S calculations were completed in Excel and PCA using SPSS. Interpolation data for rastering was carried out using ArcMap10.5.

4. Multifractal Modeling Methods

The C-A and N-S fractial models were used to separate populations in the geochemical data. Although such hard methods are used in the separation of geochemical populations, they are inefficient in recognizing settled and composite anomalies (Zuo and Wang, 2016). As for the soft threshold techniques, they applied spectrum-area (S-A) model and singularity mapping (SM). However, SM method has been widely used while returning robust meaningful results during statistical treatment of geochemical data (Zuo et al., 2013). On the other hand, the soft techniques are filtering methods and unearth the weak and complex geochemical signatures camouflaged by extreme values in the area under investigation (Parsa et al., 2017*b*). It is suggested that the soft-threshold techniques may first be used to increase ability of anticipating the

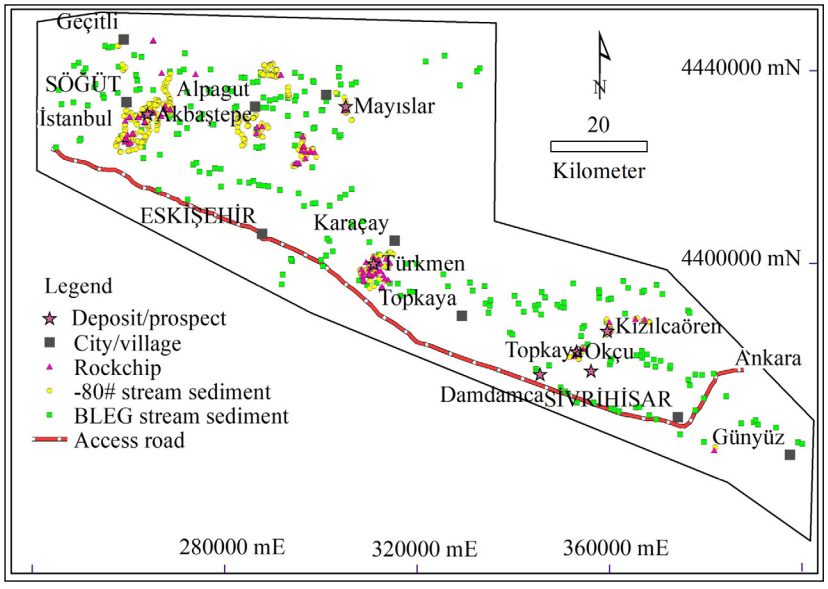

Figure 2- Location of major mineral deposits and prospects along with sampling sites for BLEG stream sediments, <180µm stream sediments and rock chips.

geochemical signatures and thereafter, hard-threshold techniques are used for the separation of multifractal geochemical anomalies. The singularity processes related to mineralizing events are, by definition, associated with accumulation of highly elevated metal concentrations within a narrow spatial-temporal interval (Halsey et al., 1986). More specifically, weak anomalies, which were not recognized because of the influences of strong background deviations or deep burial (Wang et al., 2018) can be robustly delineated. Cheng (2007) also strongly emphasized that the concept of singularity and the singularity technique are useful in delineating anomalies stemmed from mineralization and thereby predicting the locations of undiscovered ore deposits. Theory and concept of the SI (Singularity index) fractal method are described by numerous authors (Halsey et al., 1986; Cheng, 2007; Zuo and Wang, 2016; Parsa et al., 2017*a*; Yılmaz et al., 2019) and therefore, it is not necessary to repeat them in hereat.

5. Results

5.1. Delineation of BLEG and <180µm Stream Sediment Geochemical Anomalies

5.1.1. Descriptive Statistics

Histograms and Q-Q plots of BLEG Au and Ag in BLEG and Au, Ag, Cu, Pb, Zn, As and Sb in the <180µm stream sediment, along with key statistical parameters are presented in the Supplement (Supplementary Table 1 and Figures 1, 2 and 3).

5.1.2. Concentration-Area (C-A) Fractal Statistics

If the study area is treated as one mineral district without considering the effects of changing geology on geochemical background weak geochemical anomalies would not be recognized by means of Inverse Distance Weighting (IDW) because they will be camouflaged within the background variance (Arias et al., 2012). Based on log-log plots of element concentrations versus cell area with values greater than a concentration value (Figure 3) C-A plots for

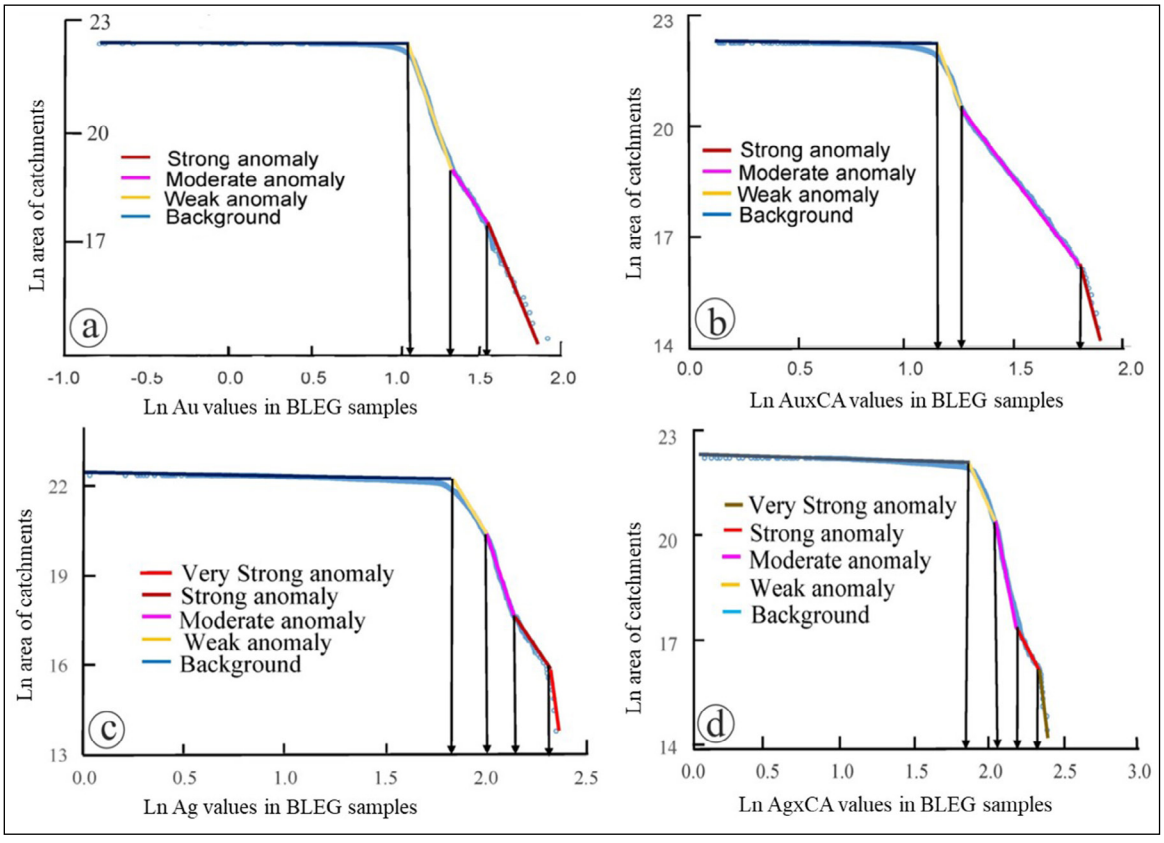

Figure 3- Ln-transformed C-A fractal model of ; a) Au, b) AuxCA; c) Ag and, d) AgxCA in BLEG samples.

BLEG Au and AuxCA may be modeled with four (4) straight lines segments whereas C-A plots for BLEG Ag and AgxCA can be modeled with five (5) straight lines segments. For Au and AuxCA (Figure 3a, b) the left-hand line segment represents backgrounds whereas the two middle line segments represent low to moderate anomalies and the right-hand line segments represent strong anomalies (Figure 3a, b). For Ag and AgxCA (Figure 3c, d) the left-hand line segment represents backgrounds whereas the three middle line segments (Figure 3c, d) represent low to strong anomalies and the right-hand line segments represents very strong anomalies. Figure 4 shows spatial distribution of BLEG Au, AuxCA, Ag and AgxCA background, weak, moderate, strong and very strong anomalies defined by C-A fractal modeling (Figure 3) and their relationship to already known deposits/prospects. As is shown in Figure 4, moderate Au and AuxCA anomalies encompass whole deposits/prospects (Figure 4c, d) whereas strong and very strong Ag and AgxCA anomalies (Figure 4c, d) cover 85% of the deposits/prospects.

5.1.3. Spatial Patterns of Multi-Element Geochemical Signatures Using C-A Statistics Model

In this study in order to extract enhanced multi-element geochemical signatures, ordinary PC as a multivariate analysis tool was applied to log-transformed data of 7 elements including Au, Ag, As, Sb, Cu, Pb and Zn from <180µm stream sediments. Geochemical associations related to different deposit types and geochemical processes in stream systems may be obtained using PC, some of which may be interpreted as pathfinders for the deposit type including Au, Ag, As, Sb, Cu, Pb and Zn from <180µm stream sediments. Geochemical associations related to different deposit types and geochemical processes in stream systems may be obtained using PC, some of which may be interpreted as pathfinders for the deposit type sought. As illustrated in Table 2, three components were extracted based on the significant eigenvalues (>0.9). The PCA results demonstrated that the log-transformed <180µm stream sediments data were classified into the following two

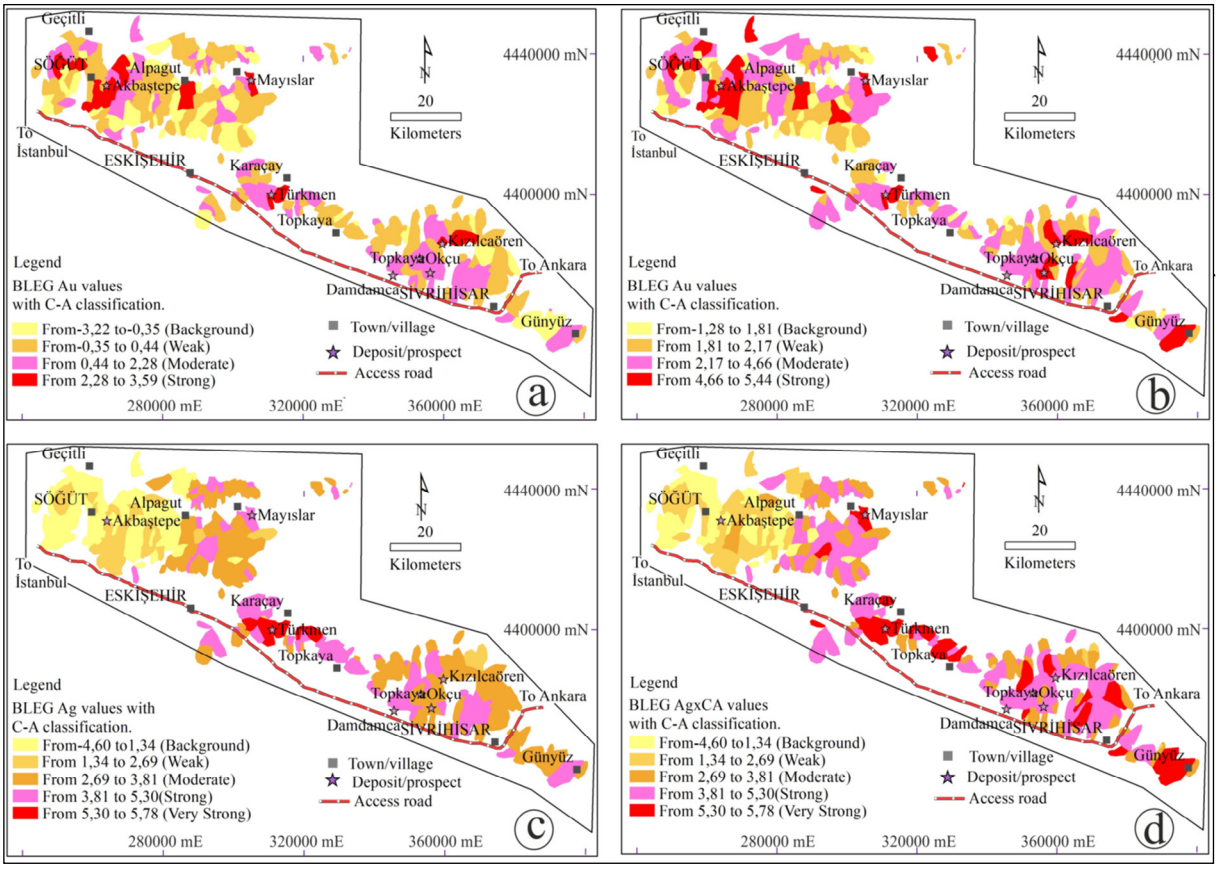

Figure 4- Geochemical maps of Ln-transformed BLEG; a) Au, b) AuxCA, c) Ag and, d) AgxCA obtained from C-A multifractal modeling.

PC2 account for ~30% and ~28% of total variability, respectively. Gold, Cu, Pb, Zn and As have significant positive PCA1 loadings and represents the effects of a mixture of orogenic, porphyry and skarn-related mineralization- in the study area. PC2 is representative of Ag and Sb mineralization. C-A and N-S fractal models were applied to the PCA scores (Figure 8) for comparison with the BLEG and BLEG Au-AgxCA and BLEGxCA Au-Ag models. The C-A fractal model indicated four BLEG Au-Ag or BLEGxCA Au-Ag populations (Figure 5). The N-S fractal model of PC1 returned 5 distinct geochemical populations of strong, moderate and weak anomalies plus background and low background for Au in <180µm data (Figure 5e, f) whereas PC2 of the <180µm stream sediment data was classified into 3 populations. Gold deposits/prospects of the area are mainly confined to the moderate to strong anomalous zones of PC1 BLEG data whereas the Akbaştepe deposit is located in the background zone of PC1 of BLEGxCA data with others occurring mostly in moderately anomalous zones (Figure 5b, d). The efficiency of PCA method is evaluated using five mineral deposits/prospects. Four of these deposits/prospects of the study area fall over the moderate to strongly anomalous zones of PC1 with positive Au-Cu-Pb-Zn-As loadings ≥ 0.5 (80% efficiency) whereas PC2 has 40% efficiency (Figure 5e-h). From geological index point of view both principal components represent Au mineralization in the area and anomalous contents of these components coincide with metamorphic (i.e. Akbaştepe) and ophiolitic rock (i.e. Mayıslar, Türkmen) types that host Au deposits and base metal prospects, respectively.

5.1.4. Spatial Patterns of Mono-Element Geochemical Signatures Using C-A and N-S Statistics Model in BLEG and <180µm Stream Sediment Data.

To augment the geochemical characteristics, the singularity mapping has been implemented to the geochemical results of BLEG and <180µm stream sediment samples. Five window sizes with minimum size of *ri* = 500 m and an interval of 500 m were used to determine singularity indices in the study area and the singularity index (α values) specific to each catchment basins obtained (Yılmaz et al., 2019). Gold and AuxCA α values ranged from 1.13 to 2.66 and 1.17 to 3.26, respectively whereas for Ag and AgxCA ranged from 1.17 to 3.27 and 0.95 to 3.62, respectively. The C-A fractal model of singularity indexes (Figure 6) indicated four distinct Au geochemical populations for BLEG Au data (Figure 6a). Likewise, the c-a fractal model has identified 5 geochemical groups ranging from strong through moderate to weak anomalies as well as background and low backgrounds for AuxCA, Ag and AgxCA (Figure 6b, c, d). Figure 6e, f, g, h also illustrates the areal dispersal of identified geochemical groups. Known gold mineralizations in the study area are confined to the strong and moderate Au and AuxCA BLEG anomaly zones (Figure 6e, f). Singularity anomaly patterns coincide much on pointing to mineralization and carbonate-mica altered metamorphic rocks in the western part (Akbaştepe/Söğüt), argillic-chlorite-talc-altered ophilites in the central part (Türkmen) and argillic-altered high-pressure metamorphic rocks in the eastern part (Topkaya, Damdamca, Okçu, Kızılören) of the study area.

Table 2- Rotated component matrix PCA on Ln-logarithmically transformed data. Loadings in bold exhibit significant geochemical indicators.

Element	PC1	PC2	PC3
Au	0.501	–0.398	0.448
Ag	–0.11	0.752	0.228
Cu	0.683	0.039	0.381
Pb	0.522	–0.654	–0.24
Zn	0.810	0.242	0.094
As	0.603	0.259	–0.651
Sb	0.290	0.813	–0.023
Eigenvalue	2.206	1.338	0.901
Var.%	29.725	27.711	12.705
Var.% cum.	29.725	57.435	70.141

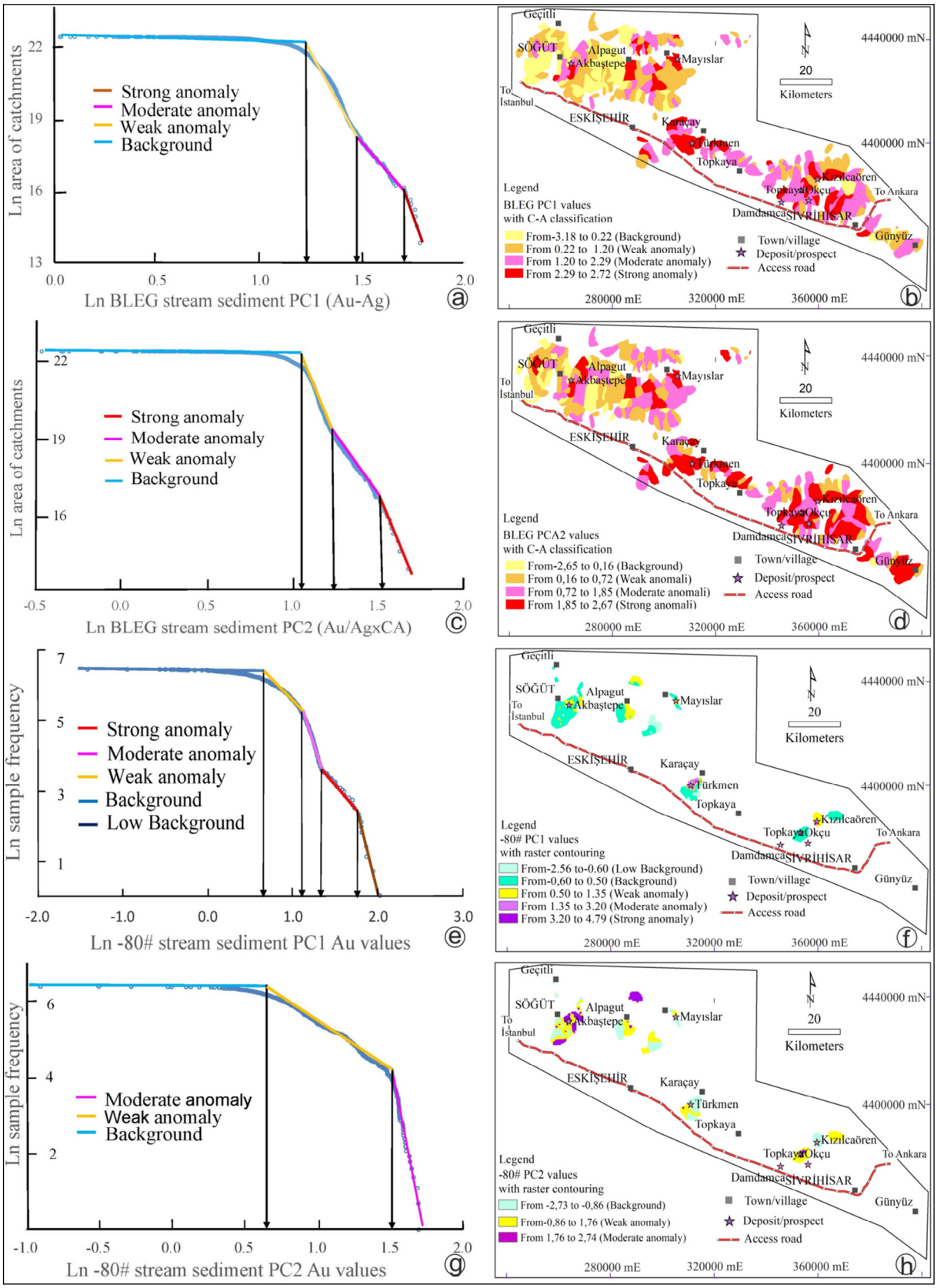

Figure 5- a), b) PC1 with fractal models and delineated geochemical anomaly population maps of Au, c), d) AuxCA in BLEG samples, e), f) PC1 and PCA2 with fractal models and delineated geochemical anomaly population maps of loaded Au+Cu+Pb+Zn+As and, g), h) Ag+Sb in <180µm stream sediment samples.

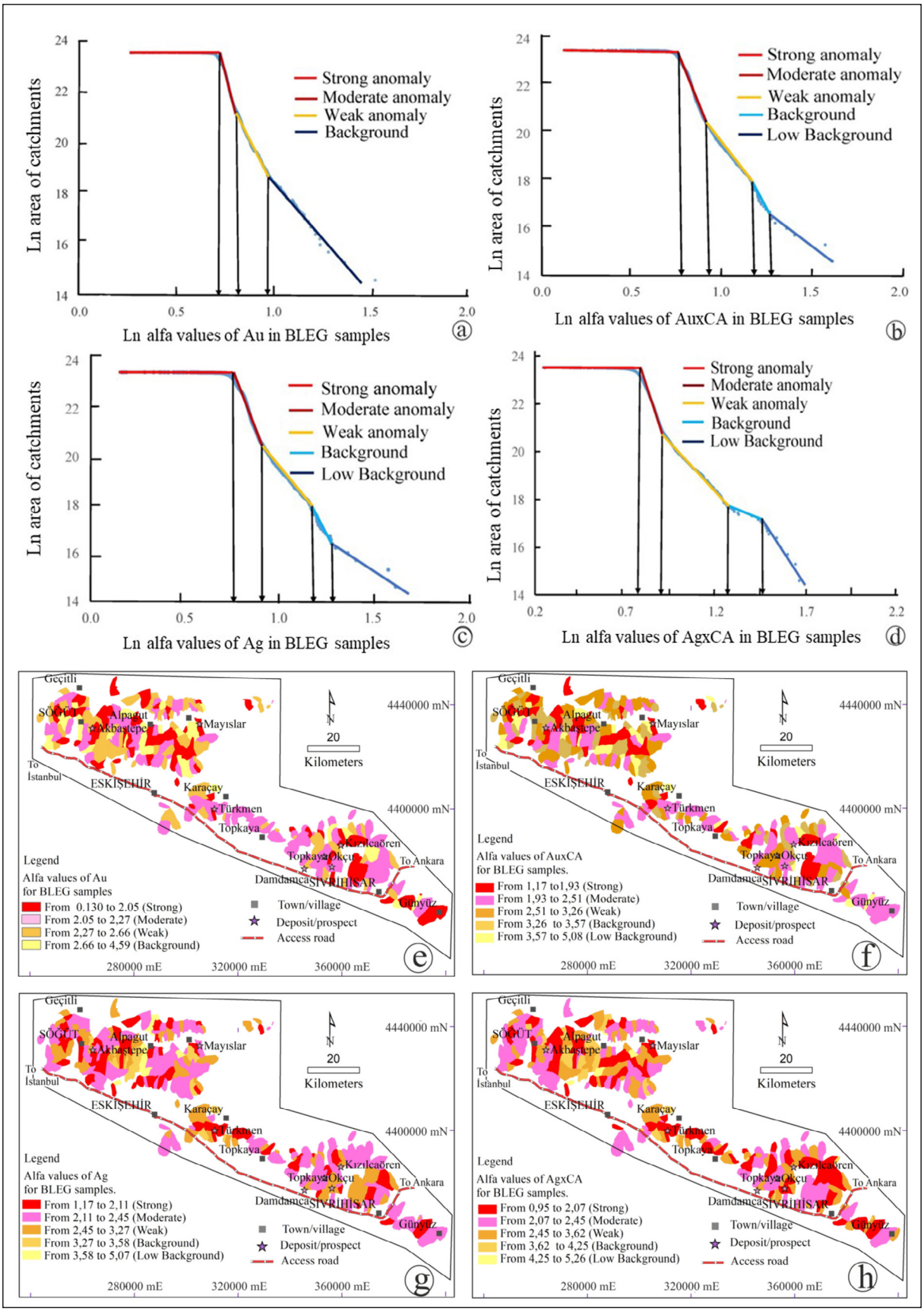

Figure 6- C-A fractal model applied to singularity indexes of; a) Au, b) AuxCA, c) Ag, d) AgxCA, e) delineated geochemical anomaly population of Au, f) AuxCA, g) Ag and h) AgxCA in BLEG samples.

5.1.5. Delineation of <180µm Stream Sediment Geochemical Anomalies

<180 um stream sediment samples were analyzed for Au, Cu, Pb, Zn As and Sb. The descriptive statistics of these elements has shown that they have positively skewed distributions (Supplementary Table 1) and thus they likely contain multiple populations. Therefore, multifractal analysis was implemented to delineate geochemical populations of these elements, which are related to mineralization. The procedure as applied to BLEG data, the results of geochemical analyses of <180µm stream sediments were initially subjected to singularity multifractal technique, with the window and interval size similar to procedure as applied to the BLEG data. To model the areal dispersion of the SI α values, a square window-based singularity mapping technique was applied as individual samples cannot be directly linked to unique catchment basins. Hence the N-S fractal model was used for the <180µm data. Four different classes of geochemical signatures of Au, As, Sb were obtained using N-S fractal model (Figure 7a, f, g) whereas the 5 geochemical populations were received for the geochemical signature of Ag, Cu, Pb and Zn in stream sediment data (Figure 7b c, d, e). The geographical dispersion maps of <180µm stream sediment α-Au, α-Cu, α-Ag, α-Pb, α-Zn, α-As and α-Sb shows the anomalies with low singularity values (Figure 8). Akbaştepe, Mayıslar, Türkmen, Okçu and Kızılcaören deposits fall over the areas with low α-Au, α-Ag, α-Zn singularity values whereas Türkmen base metal deposit is defined by high α-Au, α-Cu, α-Ag, α-Pb, α-Zn, α-As and α-Sb singularity values. To quantitatively measure the geographical correlation between areas with α and the locality of known Au deposits, the singularity maps of Au, Ag, Cu, Pb, Zn, As and Sb (Figure 8a-g), and the α values were recategorized implementing the N-S fractal model. The known gold deposits were nearly related to the lower α values (mostly less<2.2) of Au, Ag, Cu, Pb, Zn, As and Sb (Figure 8) despite of the slightly differing geographic distribution of Au, Cu, Pb, Zn, As and Sb anomalies. Besides, 100% (5), 100% (5), 60% (3), 80% (4), 100% (5), 100% (5), 60% (3) of known deposits coincide with the moderate to strong anomalies of Au, Ag, Cu, Pb, Zn, As and Sb, respectively (Figure 9). This suggests that Au, Ag, Pb, Zn and As are suitable pathfinder elements in the study area as the singularity mapping technique may recognize precious/base metal deposits/prospects.

5.1.6. Verification of the Anomalies Delineated

Figure 9 shows the efficiency assessment of the delineated BLEG and <180µm stream sediment geochemical anomalies regarding the known gold prospects and deposits of the study area. According to Figures 3-8, >85% of known gold and base metal deposits are located within the Au, AuxCA, Ag and AgxCA based on the singularity index, C-A fractal analysis and PCA. However, these values are highly variable for <180µm stream sediment data. 100% of the known deposits are located within the anomalous zones of <180µm stream sediment Zn, As and Sb based on singularity and log-transformed data with N-S fractal modeling (Figure 9). Besides, singularity index and log-transformed data of <180µm Ag and Cu with N-S fractal modeling also returned moderate to strong anomalies encompassing 100% of the deposits and prospects. Interpretation of rock sample results verify the power of the BLEG and <180µm stream sediment sampling in accurate detection of orogenic Au-As-Sb-W (Akbaştepe), Cu-Pb-Zn-As-Mo (Mayıslar), Cu-Pb-Zn-Ag-As-Sb-Au (Türkmen) and Au-Ag deposits (west of Sivrihisar Town). The anomalous zones (strong-moderate anomaly) of BLEG Au suggest that these areas deserve additional exploration campaigns. The BLEG and <180µm stream sediment geochemical Au and Ag as well as base metal anomalies recognized are encompassed by illite-sericite-silica-bearing rocks, and therefore, are of high-priority targets for supplementary exploration in addition to the already discovered occurrences (Figures 3-8).

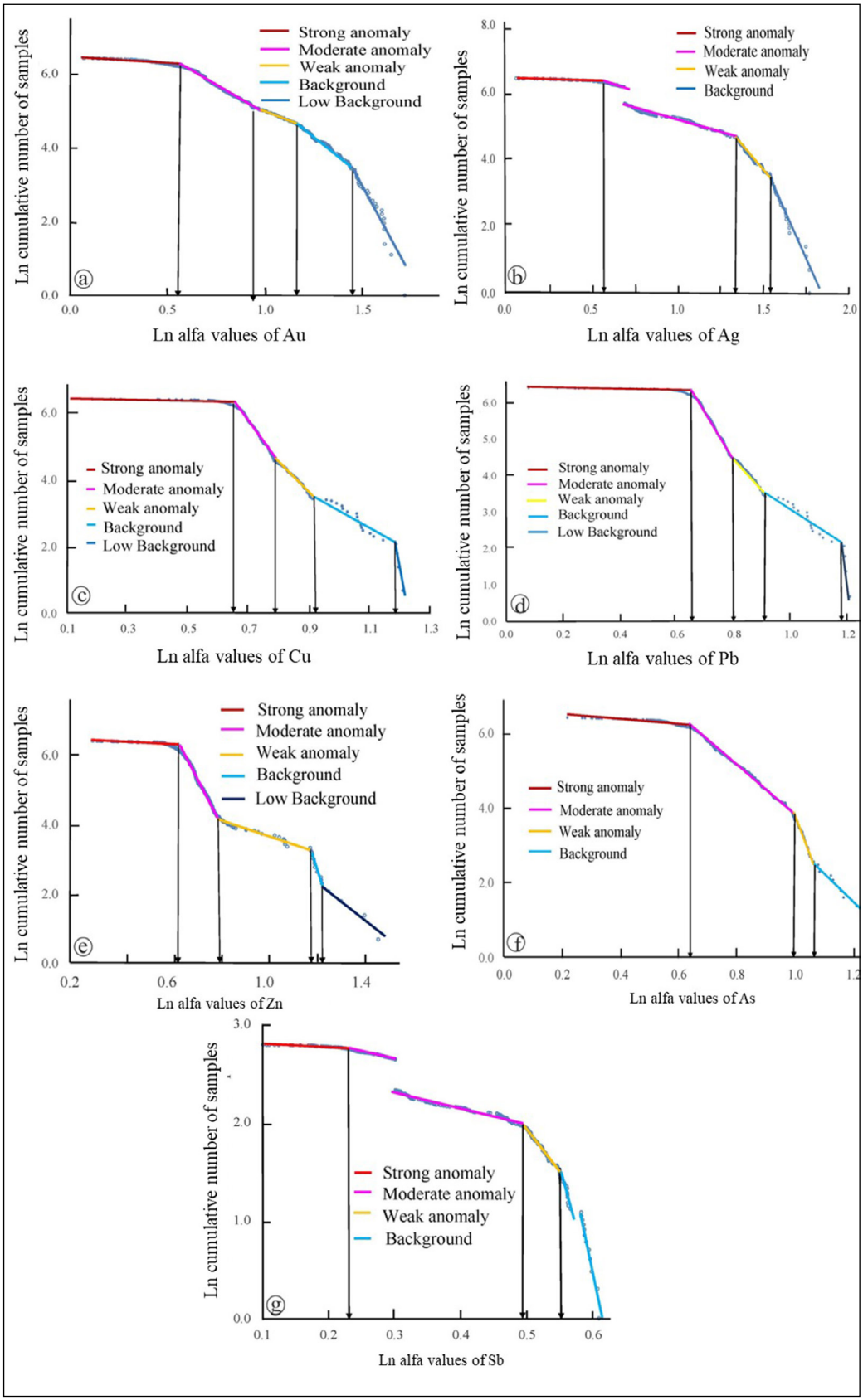

Figure 7- N-S fractal model applied to singularity indexes of; a) Au, b) Ag, c) Cu, d) Pb, e) Zn, f) As and, g) Sb in <180µm stream sediment samples.

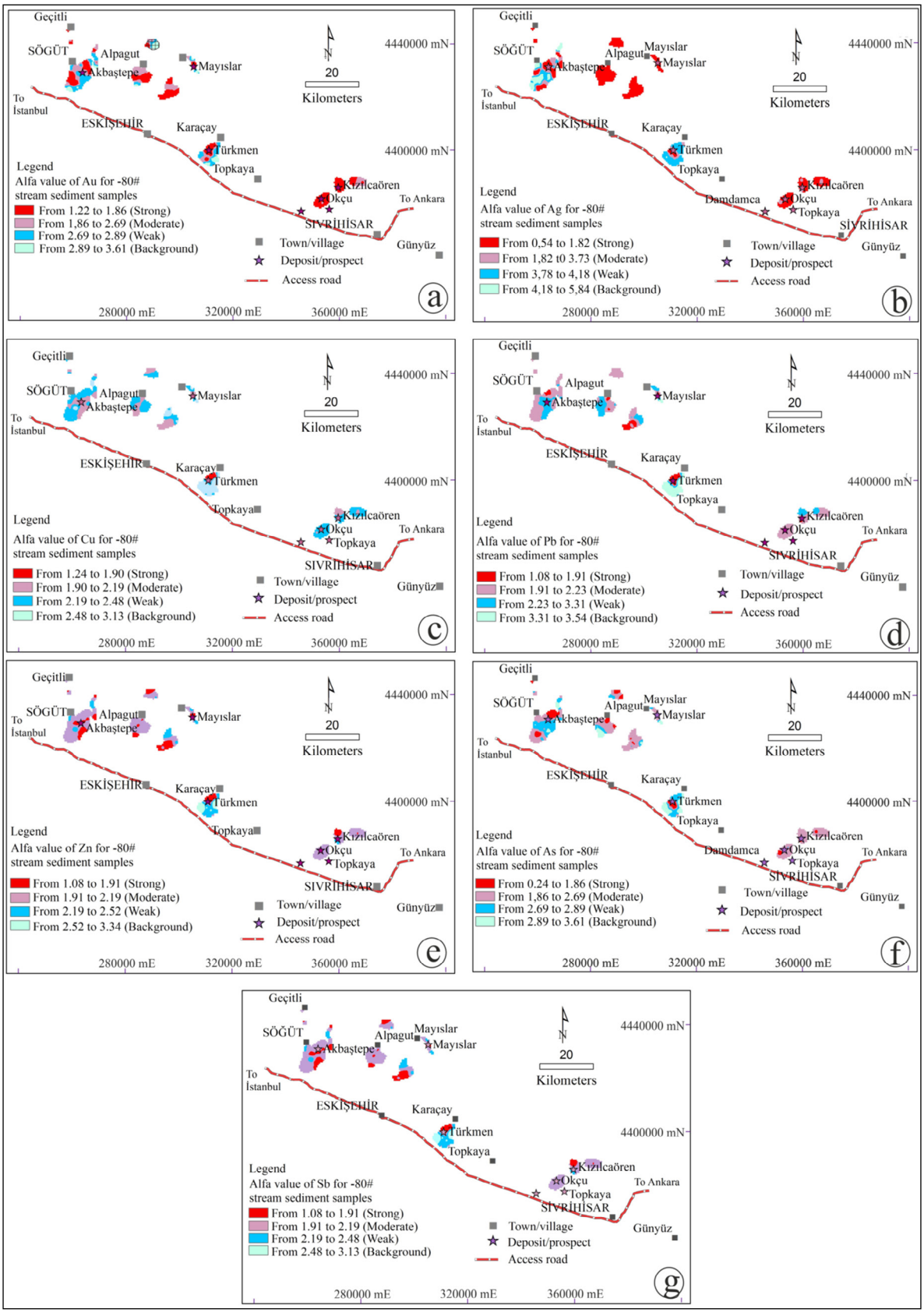

Figure 8- Raster map showing α-values of the stream sediment; a) Au, b) Ag, c) Cu, d) Pb, e) Zn, f) As and, g) Sb concentrations estimated using the window-based method.

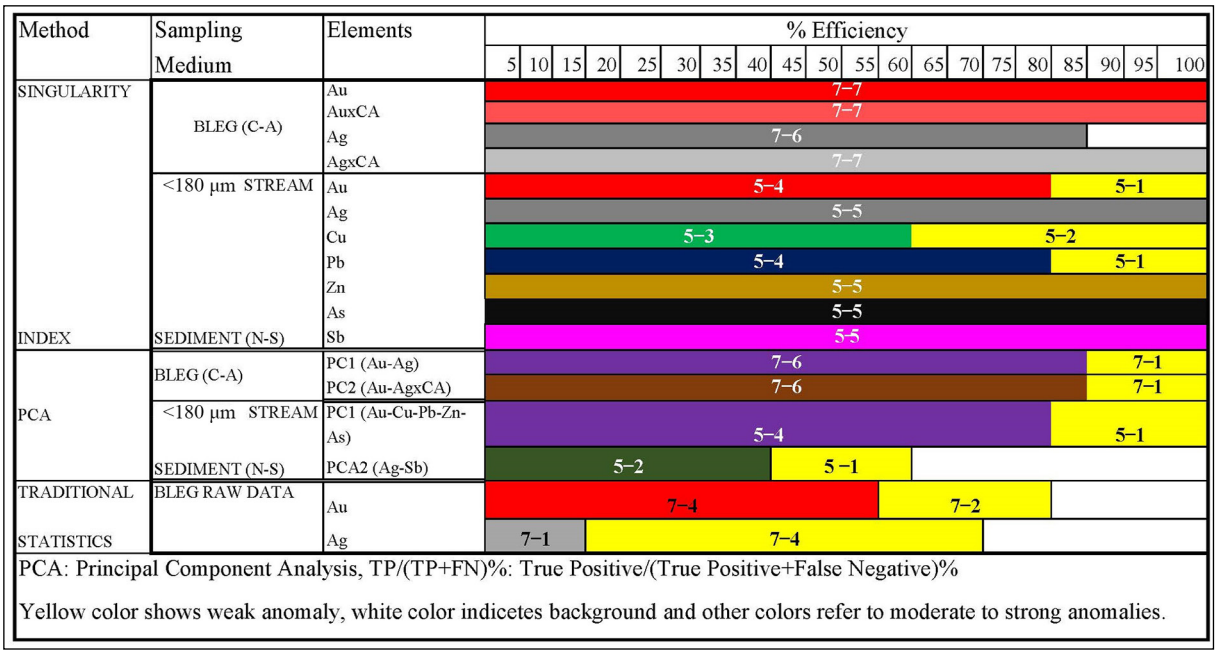

Figure 9- Agreement between geochemical anomaly classification and presence/absence of known mineral deposits or anomalous rock chip geochemistry in catchment. 7/7: number of deposits detected by stream sediment survey/Au deposits being discovered, 100%: efficiency percentage of the geochemical anomalies of stream sediment data in regard to the known gold prospects and deposits.

6. Discussion

The strength of stream sediments geochemical anomalies typically diminishes downstream due to dilution of element abundances (Parsa et al., 2017*a, b*; Yılmaz et al., 2019) in addition to errors induced by sampling and analytical errors (Parsa et al., 2016) coupled with smoothing effect by common moving average interpolation techniques (Yuan et al., 2015; Yousefi, 2017*a, b*). Nevertheless, multifractal interpolation methods (e.g., MIDW and multifractal Kriging) may use singularity and moving average interpolation to simultaneously measure local singularities and the spatial correlation between data, thereby also overcoming the smoothing effect of applying a moving average interpolation method (Cheng et al, 1999). These methods simplify the distinction of geochemical populations by enhancing geochemical anomalies and segregation from geochemical background values (Cheng et al., 2000; Yuan et al., 2015). Hard threshold techniques are not always able to identify weak anomalies (e.g., traditional statistical techniques and C-A fractal modeling), particularly in intensely altered lateritic covers (Shuguang et al., 2015). Nevertheless, when window-based contrast filtering methods, e.g., singularity mapping (Cheng et al., 1999; Cheng, 2007) are implemented as soft threshold techniques, numerous discoveries of weak geochemical anomalies have been encountered quite often (Zuo et al., 2015; Yuan et al., 2015; Yousefi, 2017*a, b*). Once the local singularity indexes (α values) are integrated in multifractal moving average interpolation, as in this study, the MIDW-interpolated geochemical data represents enhanced geochemical models, allowing for the recognition of weak anomalies. BLEG Au and Ag anomalies highly correlates with those of <180 µm stream sediment abnormalities showing the dependability of the results of sampling and analytical techniques. In addition to these, high-grade rock-chip assays as well as the discovery of mineralizations in the recognized zones of BLEG and <180µm stream sediment anomalies suggested that these BLEG and <180µm stream sediment anomaly zones without undetected mineralizations deserve further exploration. BLEG Au and Ag geochemical signatures derived from SI, C-A, N-S and PCA multifractal techniques can justify gold deposition in the study area due to the affiliation of BLEG geochemical signatures with gold mineralization (Figures 3-9). Besides, <180µm stream sediments singularity index Au and Ag geochemical anomalies have strong geographic correlation with

gold mineralization over the areas with argillic and silicic alterations. Moreover, the singularity index-based geochemical signatures of the Pb-Zn-As-Sb and C-A fractal values of Cu-Pb-Zn-As elements in <180μm stream sediment samples show strong association with gold mineralization (Figure 9). Even, <180μm stream sediments with PCA1 loadings ≥ 0.5 (Au-Cu-Pb-Zn-As) display strong association with known ore deposits at 80% efficiency level. Au and Ag geochemical anomalies, which were derived from the traditional statistical analysis of raw BLEG data had associations with known deposits with 57% and 15% underlain by moderate to weak anomalies, respectively (Supplementary Figure 3 and Figure 9). However, Log-transformed BLEG Au and Ag signatures display association with the known deposits at 100% and 30 efficiency level, respectively. It was demonstrated that IDW interpolation of Log-transformed Au anomalies derived from median +2σ, 3σ and 4σ detected all the deposits/prospects. However, multifractal analysis also generates additional moderate to strong, even weak, BLEG Au and Ag anomalies, which may be targets for discovering additional significant Au deposits (Supplementary Figure 3c, d and Figures 4-6). This shows that multifractal analysis is robust and very efficient in identifying ore-related geochemical anomalies, which have been probably missed by traditional statistical analysis. The geochemical anomalies derived from SI coupled with C-A and N-S fractal/multifractal models should be accompanied by further prospecting and structural mapping. This would probably give way to the identification of new mineralization sites encompassed by low α values <2.

Acknowledgements

We would like to express our appreciation to Eurogold Madencilik/Normandy Mining Ltd., Türkiye for generous financial support to the project during Hüseyin YILMAZ's presence in Eurogold as Exploration Manager. Anonymous reviewers are thanked for their invaluable comments in improving the quality of this paper.

References

Afzal, P., Khakzad, A., Moarefvand, P., Omran, N. R., Esfandiari, B., Alghalandis, Y. F. 2010. Geochemical anomaly separation by multifractal modeling in Kahang (GorGor) porphyry system, Central Iran. Journal of Geochemical Exploration 104, 34–46.

Afzal, P., Alghalandis, Y. F., Khakzad, A., Moarefvand, P., Omran, N. R. 2011. Delineation of mineralization zones in porphyry Cu deposits by fractal concentration–volume modeling. Journal of Geochemical Exploration 108, 220–232.

Afzal, P., Ahari H. D, Omran, N. R, Aliyari F. 2013. Delineation of gold mineralized zones using concentration–volume fractal model in Qolqoleh gold deposit, NW Iran. Ore Geology Reviews 55, 125–133.

Agterberg, F. P., Bonham-Carter, G. F., Wright, D. F. 1990. Statistical pattern integration for mineral exploration. Computer applications in resource exploration and assessment for minerals and petroleum. Pergamon, Elmsford.

Ahmadi, N. R, Afzal, P., Yasrebi, A. B. 2021. Delineation of gas content zones using N-S fractal model in coking coal deposits. Journal of Mining and Environment 12, 181-189.

Ak Yatırım. 2018. Ak Yatırım Madencilik şirket raporu, 4 (unpublished).

Aliyari, F. P., Afzal, P., Lotfi, M., Shokri, S. H., Feizi, H. 2020. Delineation of geochemical haloes using the developed zonality index model by multivariate and fractal analysis in the Cu–Mo porphyry deposits. Applied Geochemistry 121, 104694.

Altıner, D., Koçyiğit, A., Farinacci, A., Nicossia, U., Conti, M. A. 1991. Jurassic, Lower Cretaceous stratigraphy and paleogeographic evolution of the southern part of north-western Anatolia. Geologica Romana 28, 13-80.

Arias, M., Gumiel, P., Martín-Izard, A. 2012. Multifractal analysis of geochemical anomalies: a tool for assessing prospectivity at the SE border of the Ossa Morena Zone, Variscan Massif (Spain). Journal of Geochemical Exploration 122, 101-112.

Bonham-Carter, G. F., Rogers, P. J., Ellwood, D. J. 1987. Catchment basin analysis applied to surficial geochemical data, Cobequid Highlands, Nova Scotia. Journal of Geochemical Exploration 29, 259-278.

Carranza, E. J. M. 2010*a*. Catchment basin modelling of stream sediment anomalies re-visited: incorporation of EDA and fractal analysis. Geochemistry: Exploration, Environment, Analysis 10, 365-381.

Carranza, E. J. M. 2010*b*. Mapping of anomalies in continuous and discrete fields of stream sediment geochemical landscapes. Geochemistry: Exploration, Environment, Analysis 10, 171–187.

Cheng, Q. 2007. Mapping singularities with stream sediment geochemical data for prediction of undiscovered mineral deposits in Gejiu, Yunnan Province, China. Ore Geology Reviews 32, 314-324.

Cheng, Q., Agterberg, F. P., Ballantyne, S. B. 1994. The separation of geochemical anomalies from background by fractal methods. Journal of Geochemical Exploration 51, 109-130.

Cheng, Q., Agterberg, F. P., Bonham-Carter, G. F. 1996. A spatial analysis method for geochemical anomaly separation. Journal of Geochemical Exploration 56, 183–195.

Cheng, Q., Xu, Y., Grunsky, E. 1999. Integrated spatial and spectral analysis for geochemical anomaly separation. Proceeding of the Fifth Annual Conference of the International Association for Mathematical Geology, Trondheim, Norway 6–11th August.

Cheng, Q., Xu, Y., Grunsky, E. C. 2000. Integrated spatial and spectrum method for geochemical anomaly separation. Natural Resources Research 9, 43–52.

Daneshvar, S. L. 2017. Delineation of enriched zones of Mo, Cu and Re by concentration volume fractal model in Nowchun Mo-Cu porphyry deposit, SE Iran. Iranian Journal of Earth Sciences 9, 64- 72.

Eurogold, 1996. Review report on gold anomalies and prospects generated between 1991 and 1996 in western Turkey, Unpublished Company Report, 200.

Govett, G. J. S., Goodfellow, W. D., Chapman, A., Chor, C. Y. 1975. Exploration geochemistry-distribution of elements and recognition of anomalies. Mathematical Geology 7, 415–446.

Grunsky, E. C. 2007. The interpretation of regional geochemical survey data. Advances in Regional-Scale Geochemical Methods 8, 139–182.

Grunsky, E. 2010. The interpretation of geochemical survey data. Geochemistry: Exploration, Environment, Analysis 10, 27–74.

Halsey, T. C., Jensen, M. H., Kadanoff, L. P., Procaccia, I., Shraiman, B. I. 1986. Fractal measures and their singularities: the characterization of strange sets. Physics Review 33, 1141–1151.

Hawkes, H. E. 1976. The downstream dilution of stream sediment anomalies. Journal of Geochemical Exploration 6, 345–358.

Howarth, R. J. 1983. Mapping. Statistics and Data Analysis I Geochemical Prospecting, Handbook of Exploration Geochemistry 2. Elsevier, Amsterdam, 111–205.

Koza Gold. 2013. Koza Gold Company activity report, 54 (unpublished).

Koza Gold. 2014. Koza Gold Company activity report, 63 (unpublished)

Koza Gold. 2016. Koza Gold Company activity report, 97 (unpublished)

Luz, F., Mateus, A., Matos, J. X., Gonçalves, M. A. 2014. Cu-and Zn-soil anomalies in the NE border of the South Portuguese Meier Zone (Iberian Variscides, Portugal) identified by multifractal and geostatistical analyses. Natural Resources Research 23, 195-215.

Mandelbrot, B. B. 1983. The Fractal Geometry of Nature. Freeman, New York, 495.

Mirzaie, M., Afzal, P., Adib, A., Rahimi, E., Mohammadi, G. 2020. Detection of zones based on ore and gangue using fractal and multivariate analysis in Chah Gaz iron ore deposit, Central Iran. Journal of Mining and Environment 11, 453-466.

MTA. 1965. Tungsten and molybdenum deposits of Turkey. General Directorate of Mineral Research and Exploration Publications No. 128, Ankara, Turkey.

MTA. 1970. Arsenic, mercury, antimony and gold deposits of Turkey. General Directorate of Mineral Research and Exploration Publication No. 129, Ankara, Turkey.

MTA. 2002. 1:500000 Geological map of Turkey. General Directorate of Mineral Research and Exploration, Ankara, Turkey.

Okay, A. I., Satır, M. 2000. Coeval plutonism and metamorphism in a latest Oligocene metamorphic core complex in northwest Turkey. Geological Magazine 137, 495–516.

Okay, A. I., Satır, M., Maluski, H., Siyako, M., Monie, P., Metzger, R., Akyüz, S. 1996. Paleo- and Neo-Tethyan events in northwest Turkey: geological and geochronological constraints. Tectonics of Asia. Cambridge University Press, 420–441.

Özgenç, I. 1993. Kızılcaören (Sivrihisar-Eskişehir) karbotermal bastneazit-fluorit-barit yatağının jeolojisi ve nadir toprak element jeokimyası. Geological Bulletin of Turkey 36, 1–11.

Parlak, B., Sayılı, S. 2012. Fluid inclusion data on quartz and calcite in alteration zones of polymetallic mineralizations at Mayıslar Area (Sarıcakaya-Eskişehir, Turkey). Geological Bulletin of Turkey 55, 111−132.

Parsa, M., Maghsoudi, A., Ghezelbash, R. 2016. Decomposition of anomaly patterns of multi-element geochemical signatures in Ahar area, NW Iran: a comparison of U-spatial statistics and fractal models. Arabian Journal of Geosciences 9, 1-16.

Parsa, M., Maghsoudi, A., Yousefi, M., Sadeghi, M. 2017*a*. Multifractal analysis of stream sediment geochemical data: implications for hydrothermal nickel prospection in an arid terrain, eastern Iran. Journal of Geochemical Exploration 18, 305-317.

Parsa, M., Maghsoudi, A., Yousefi, M., Carranza, E. J. M. 2017*b*. Multifractal interpolation and spectrum–area fractal modeling of stream sediment geochemical data: implications for mapping exploration targets. Journal of African Earth Sciences 128, 5-15.

Ren, L., Cohen, D. R., Rutherford, N. F., Zissimos, A. M., Morisseau, E. G. 2015. Reflections of the geological characteristics of Cyprus in soil rare earth element patterns. Applied Geochemistry 56, 80–93.

Sadeghi, B., Madani, N., Carranza, E. J. M. 2015. Combination of geostatistical simulation and fractal modeling for mineral resource classification. Journal Geochemical of Exploration 149, 59–73.

Shen, W., Cohen, D. R. 2005. Fractally invariant distributions and an application in geochemical exploration. Mathematical Geology 37, 895–909.

Shuguang, Z., Kefa, Z., Yao, C., Jinlin, W., Jianli, D. 2015. Exploratory data analysis and singularity mapping in geochemical anomaly identification in Karamay, Xinjiang, China. Journal of Geochemical Exploration 154, 171-179.

Sinclair, A. J. 1991. A fundamental approach to threshold estimation in exploration geochemistry: Probability plots revisited. Journal of Geochemical Exploration 41, 1–22.

Wang, W., Cheng, Q., Zhang, S., Zhao, J. 2018. Anisotropic singularity: A novel way to characterize controlling effects of geological processes on mineralization. Journal of Geochemical Exploration 189, 32–41

Yasrebi, A. B., Hezarkhani, A. 2019. Resources classification using fractal modelling in Eastern Kahang Cu-Mo porphyry deposit, Central Iran. Iranian Journal of Earth Sciences 11, 56-67.

Yılmaz, H. 2003. Geochemical exploration for gold in western Turkey: success and failure. Journal of Geochemical Exploration 80, 117-135.

Yılmaz, H., Mahyar, Y., Parsa, M., Sonmez, F. N., Maghsoodi, A. 2019. Singularity mapping of bulk leach extractable gold and -80# < 180µm stream sediment geochemical data in recognition of gold and base metal mineralization footprints in Biga Peninsula South, Turkey. Journal of African Earth Sciences 153, 156-172.

Yousefi, M. 2017*a*. Analysis of zoning pattern of geochemical indicators for targeting of porphyry Cu mineralization: A pixel-based mapping approach. Natural Resources Research 26, 429–441.

Yousefi, M. 2017*b*. Recognition of an enhanced multi-element geochemical signature of porphyry copper deposits for vectoring into mineralized zones and delimiting exploration targets in Jiroft area, SE Iran. Ore Geology Reviews 83, 200-214.

Yuan, F., Li, X., Zhou, T., Deng, Y., Zhang, D., Xu, C., Zhang, R., Jia, C., Jowitt, S. M. 2015. Multifractal modeling-based mapping and identification of geochemical anomalies associated with Cu and Au mineralization in the NW Junggar area of northern Xinjiang Province, Gangdese Belt, Tibet (China). Journal of Geochemical Exploration 154, 252-264.

Zadmehr, F., Shahrokhi, S. V. 2019. Separation of geochemical anomalies by concentration-area and concentration-number methods in the Saqez 1/100.000 sheet. Iranian Journal of Earth Sciences 11, 196-204.

Zuo, R. 2011. Identifying geochemical anomalies associated with Cu and Pb–Zn skarn mineralization using principal component analysis and spectrum–area fractal modeling in the Gangdese Belt, Tibet (China). Journal of Geochemical Exploration 111, 13–22.

Zuo, R., Wang, J. 2016. Fractal/multifractal modeling of geochemical data: a review. Journal of Geochemical Exploration 164, 33-41.

Zuo, R., Xia, Q., Wang, H. 2013. Compositional data analysis in the study of integrated geochemical anomalies associated with mineralization. Applied Geochemistry 28, 202-211.

Zuo, R., Xia, Q., Wang, H. 2015. Compositional data analysis in the study of integrated geochemical anomalies associated with mineralization. Applied. Geochemistry 28, 202–211.

Supplementary Material

1. Descriptive Statistics

The skewness and kurtosis of the raw Au and Ag concentrations in the BLEG stream sediments are 8.9 and 10.3, and 102 and 122 whereas these are 4.9 and 7.4, and 28.4 and 58.8, respectively for AuxCA and AgxCA (Figure 1). The skewness and kurtosis of the Ln Au and Ln Ag concentrations in the BLEG are 0.3 and -0.6 and, 1.8 and -0.6 respectively, indicating that the BLEG Au have slightly negative skewness and low kurtosis whereas the BLEG Ag have negative skewness and low kurtosis. Again, Ln-transformed Au and Ag data do not fully follow a normal distribution (as shown by Table 1) and histograms, and Q-Q plots in Figure 1. In addition, the histogram of the logarithmic Ag concentrations has a multimodal pattern for the BLEG (Figure 1h). These statistical characteristics may suggest that the Eskişehir-Sivrihisar region have had multiple geochemical framework and has undergone multi-geological processes, thereby displaying a complex Ag ore-formation during Eocene time. The skewness of the raw Au, Ag, Cu, Pb, Zn, As and Sb concentrations in the <180µm stream sediment data are 6.9, 5.6, 4.8, 11.1, 7.2, 7.5 and 2.7, respectively (Table 1 and Figure 1). This indicates that the data are positively skewed containing large positive tailing values with very excessive kurtosis (Au: 66.8, Ag: 43.7, Cu: 31.7, Pb: 148.1, Zn: 61, As: 84.7 and Sb: 9.1) and the data do not follow a normal distribution (as shown in the Table 1 and histograms in Figure 2 a-g). Ln Cu, Pb and Zn histograms display moderately normal and leptokurtic distributions (Figure 2h, q) with Ln Cu and As displaying negative skewness. However, Ln-transformed Au, Ag, As and Sb data do not fully follow a normal distribution (as shown in Figure 2. In and addition, the histograms of the Ln Au, Ag, Cu, Pb, Zn, As and Sb concentrations have weak to strong multimodal patterns for the <180µm stream sediments (Figure 2). These statistical characteristics as in the BLEG data imply that the Eskişehir-Sivrihisar region have had multiple geochemical framework and has undergone multi-geological processes, thereby complex ore-formations during Eocene time. As is typical for trace element geochemical data, the distributions are skewed with an overall tendency towards right, but significant deviations from ln-normality due to the complex interplay of factors such as parent lithology controlling element distributions (Reimann and Filzmoser, 2000; Ren et al., 2015). The size of BLEG Au- and Ag-anomalous areas above background generated by traditional statistics using median+2S.D (Table 1) was calculated using IDW interpolation by ArcGis 10.5 version. Maximum anomalous areas above the background for raw Au and Ag data are 266 km^2 (Figure 3a) and 31 km^2 (Figure 3b) whereas these are 2895 km^2 (Figure 3c) for Ln Au and 683 km^2 (Figure 3d) for Ln Ag, which are derived from 3580 km^2 BLEG-sampled area. The ratio of raw Au and Ag anomalous areas to that of BLEG-sampling is 1/15 and 1/115, respectively whereas these are 1/1.25 for LnAu and 1/1.4 for LnAg. However, these ratios may be decreased to 1/5 and 1/3.7 of BLEG-sampled area for LnAu and for LnAg, respectively, at median+3SD (Red highlighted areas in Figure 3c, d). Number of deposits/prospects detected by raw Au and raw Ag anomalies are 3 (45%) and 1 (15%) out of 7, respectively whereas percentage of discoveries of deposits/prospects by weak to strong LnAu and LnAg anomalies are 100 and 85%, respectively, with the majority of mineralizations covered by strong LnAu anomalies.

References

Reimann, C., Filzmoser, P. 2000. Normal and lognormal data distribution in geochemistry: death of a myth, consequences for the statistical treatment of geochemical and environmental data. Environmental Geology 39, 1001–1014.

Ren, L., Cohen, D. R., Rutherford, N. F., Zissimos, A. M., Morisseau, E. G. 2015. Reflections of the geological characteristics of Cyprus in soil rare earth element patterns. Applied Geochemistry 56, 80–93.

Table 1- Summary statistics for BLEG Au and Ag, and <180 µm Stream sediment Au, Ag, Cu, Pb, Zn, As and Sb.

BLEG							
	Au (ppb)	AuxCA	Ag (ppb)	AgxCA			
Mean	1.4	15.2	12.72	122.1			
Std. Deviation	2.9	29.2	44.64	382.5			
Skewness	8.9	4.9	10.28	7.4			
Kurtosis	101.9	28.4	121.81	58.8			
Minimum or DL	0.0	0.3	0.01	0.1			
Maximum	38.1	252.8	595.51	3763.6			
N	258	258	258	258			
<180 µm stream sediment							
	Au (ppb)	Ag (ppm)	Cu (ppm)	Pb (ppm)	Zn (ppm)	As (ppm)	Sb (ppm)
Mean	15.2	1.2	49.7	95.2	92.5	41.2	5.4
Std. Deviation	42.9	3.5	51.6	386.1	202.3	70.3	8.7
Skewness	6.9	5.6	4.8	11.1	7.2	7.5	2.7
Kurtosis	66.8	43.7	31.7	148.1	61.0	84.7	9.1
Minimum or DL	0.3	0.0	3.0	1.0	5.0	1.0	1.0
Maximum	587.0	40.1	539.2	6292.5	2441.2	1056.6	61.7
N	612	612	612	612	612	612	612

BLG: Bulk Leach Extractable Gold, CA: Concentration times area in square km, N: Number of samples, DL: Detection limit

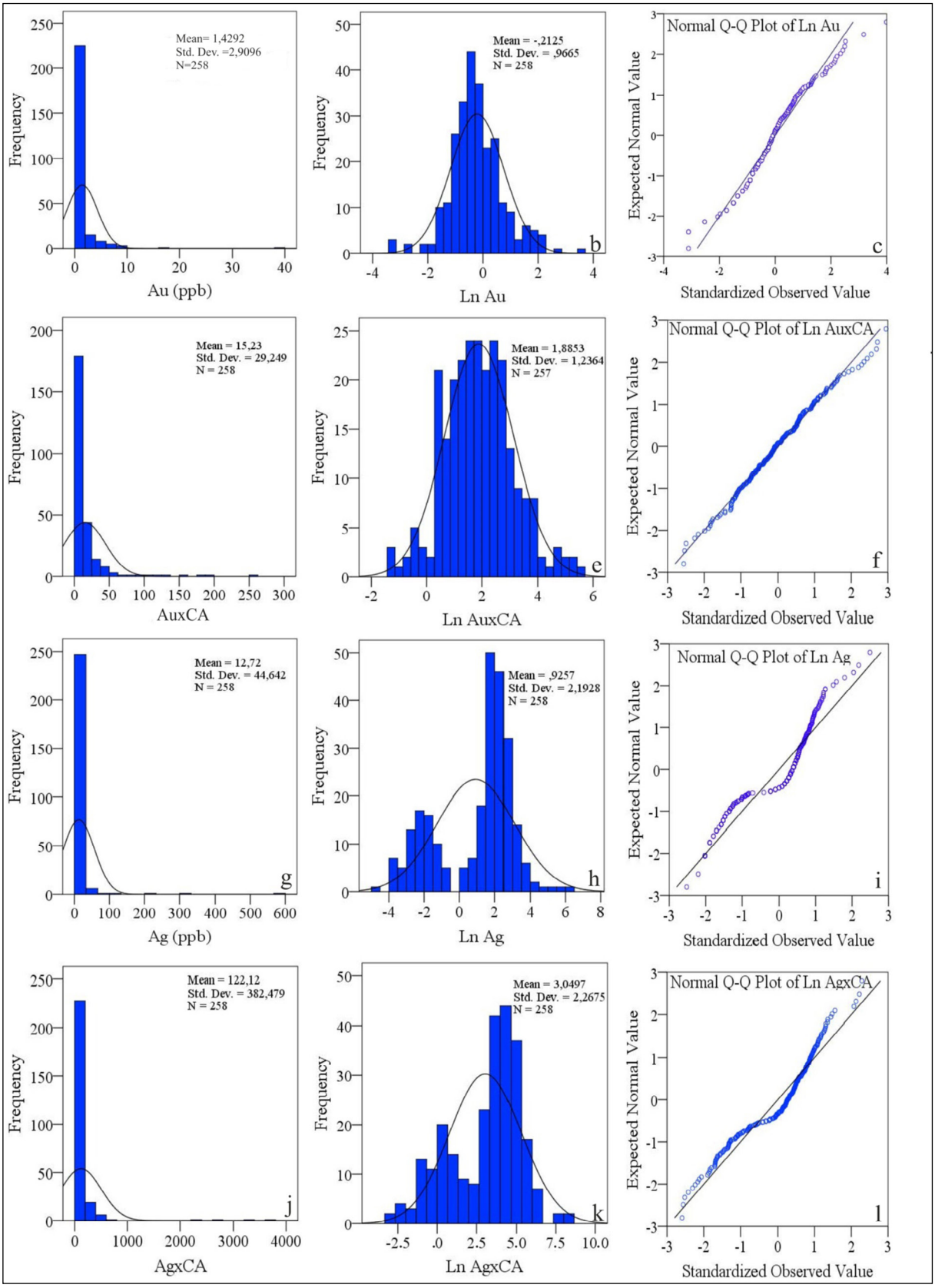

Figure 1- The Au-Ag statistical charts from the BLEG stream sediment samples in the Eskişehir-Sivrihisar region; a) the raw Au, b) Ln Au, c) Q-Q Au, d) Raw AuxCA, e) Ln AuxCA, f) Q-Q Ln Au, g) the raw Ag, h) Ln Ag, i) Q-Q Ag, j) Raw AgxCA, k) Ln AgxCA, l) Q-Q Ln AgxCA.

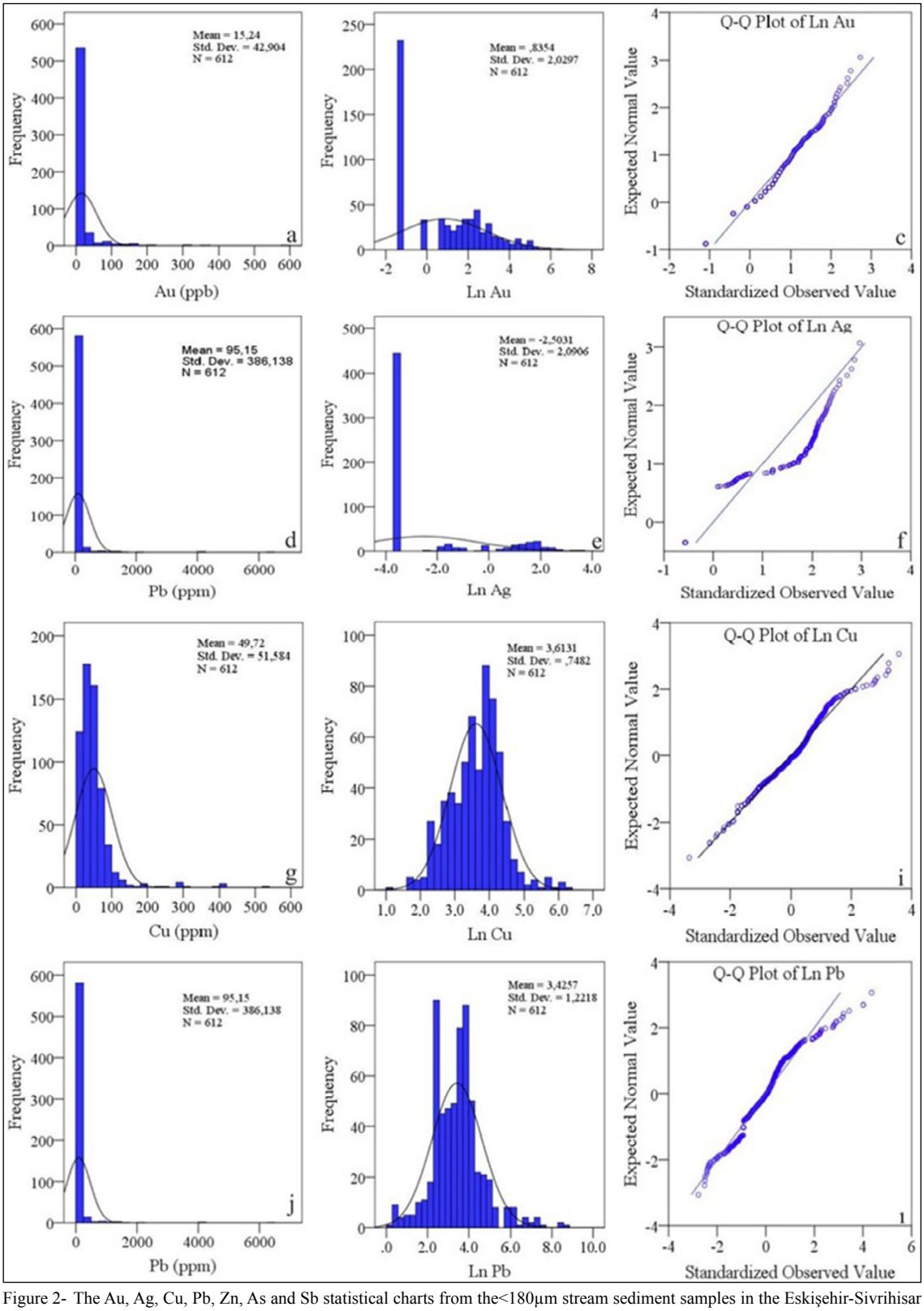

Figure 2- The Au, Ag, Cu, Pb, Zn, As and Sb statistical charts from the<180µm stream sediment samples in the Eskişehir-Sivrihisar region; a) the raw Au, b) Ln Au, c) Q-Q Au, d) Raw Ag, e) Ln Ag, f) Q-Q Ln Ag, g) the raw Cu, h) Ln Cu, i) Q-Q Cu, j) Raw Pb, k) Ln Pb, l) Q-Q Ln Pb, m) Raw Zn, n) Ln Zn, o) Q-Q Ln Zn, p) Raw As, q) Ln As, r) Q-Q Ln As, s) Raw Sb, t) Ln Sb, u) Q-Q Ln Sb.

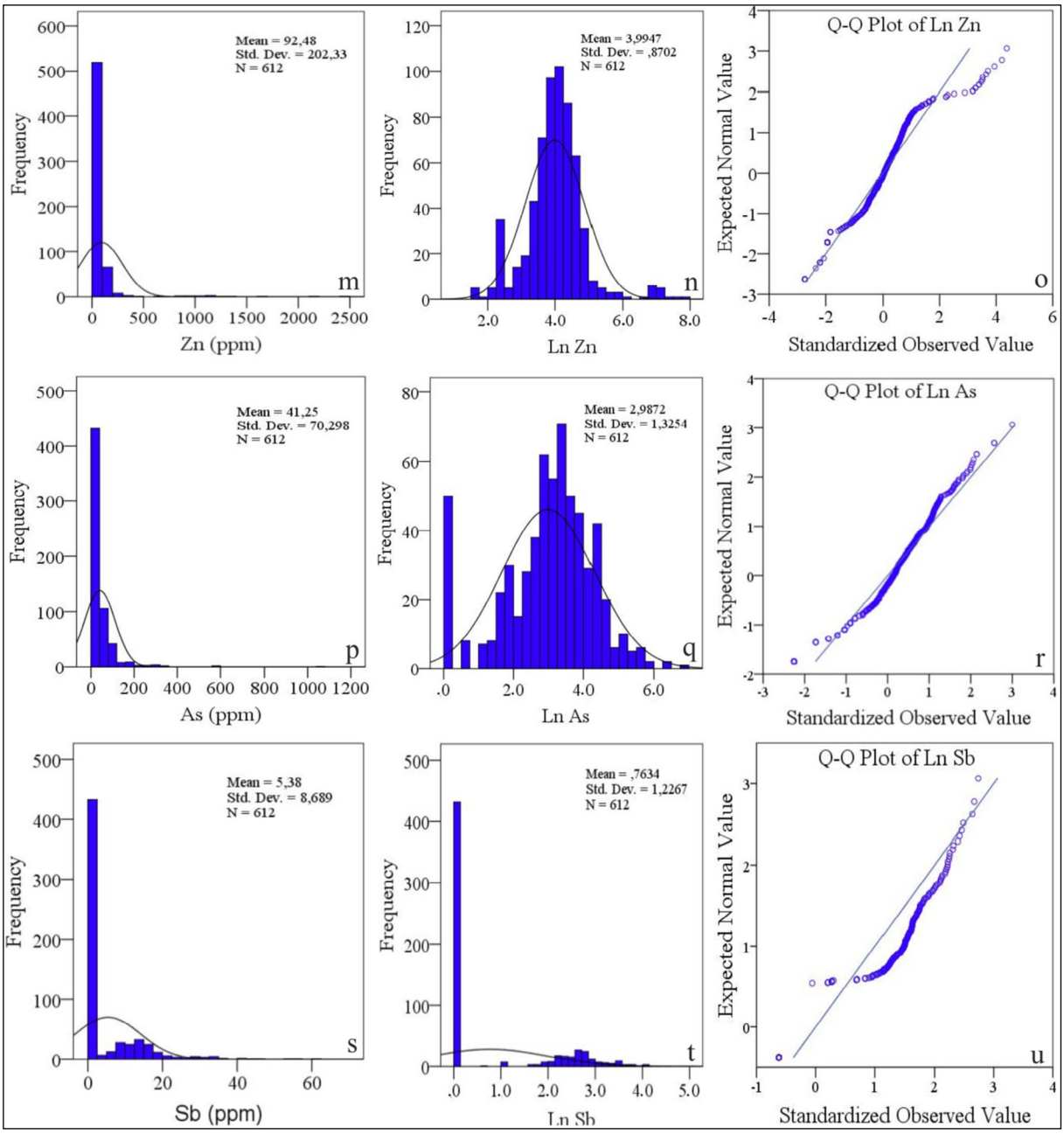

Figure 2- Continued.

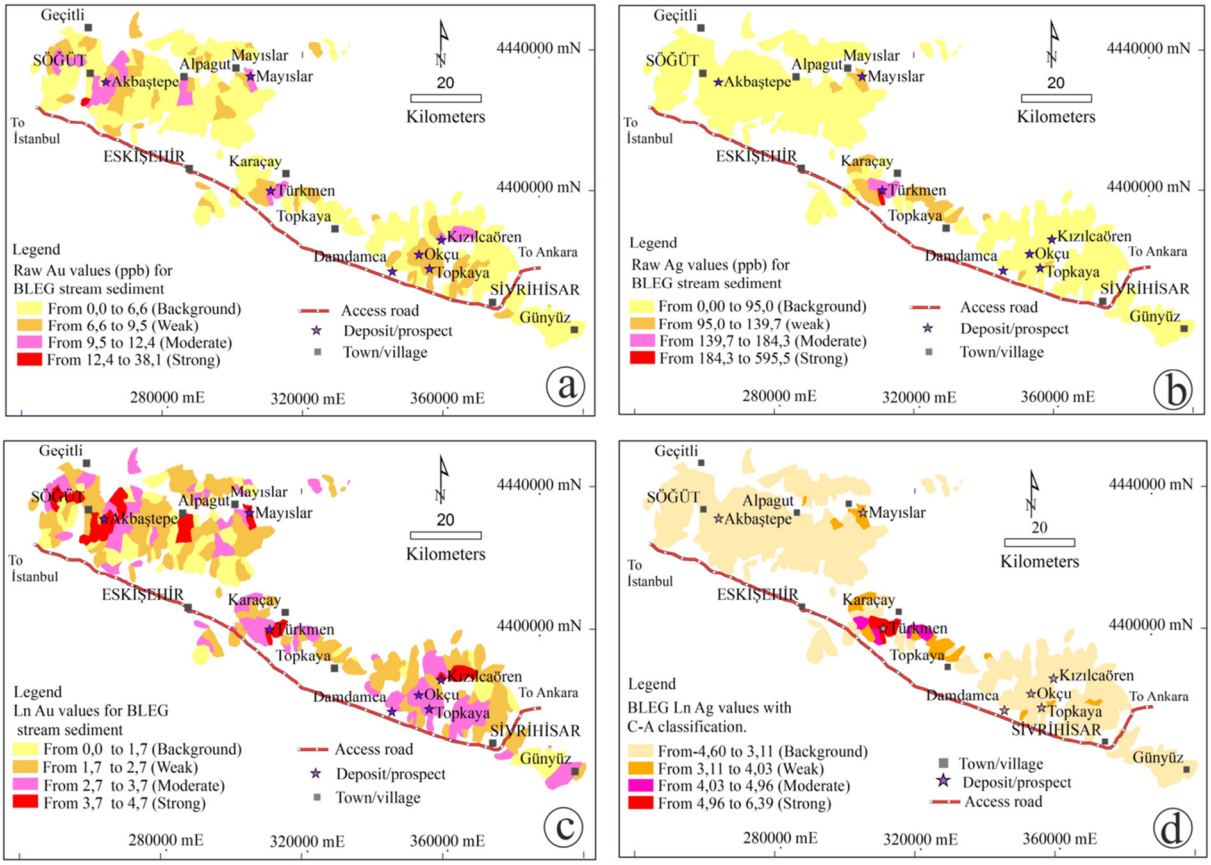

Figure 3- Areal extent of raw; a) Au-anomalous, b) Ag-anomalous areas generated by median+2S.D, and c), d) Ln-transformed Au-Ag-anomalous fields derived from median+2SD, 3SD and 4SD in the Eskişehir-Sivrihisar area. Median+1SD refers to background.